THE ROYAL SOCIETY

J. R. Soc. Interface (2004) **1**, 49–59
DOI: 10.1098/rsif.2004.0006

Optical properties of the scales of *Morpho rhetenor* butterflies: theoretical and experimental investigation of the back-scattering of light in the visible spectrum

Luca Plattner[†]

Electronics and Computer Science Department, University of Southampton, Southampton SO17 1BJ, UK

A study of the optical properties of the largely periodic microstructure occurring on the wings of the iridescent tropical butterfly *Morpho rhetenor* and responsible for its structural colouration is reported. An extensive measurement of the back-scattering of visible light from butterfly scales was performed for various angles of incidence. Efficient low-pass filter behaviour was observed for all angles of incidence and polarizations, with near-complete transmission at wavelengths above the threshold of 550 nm. The angular spread of the back-scattered light was found to be organized in lobes with total extinction of the specular reflection for all conditions of incidence. Retro-reflector behaviour was also observed for angles of incidence of 30° and above. Additionally, the role of periodic geometrical features found in the microstructure for the generation of its spectral response was analysed theoretically. Using finite-difference time-domain and near-field to far-field transformation techniques, the back-scattering of visible light by models was computed numerically and the relevance of geometrical features for the production of structural colour and diffraction was demonstrated.

Keywords: ***Morpho rhetenor*; scattering; diffraction; FDTD; spectroscopy**

1. INTRODUCTION

Through various arrangements of biological material many organisms take advantage of complex optical effects to generate or manipulate their colouration. A chromatic display based on physical mechanisms, such as interference and diffraction of light, rather than on the more conventional chemical absorption is commonly referred to as *structural colour*. The history of the scientific investigation of structural colour in nature is long and it includes the illustrious scientific figures Hooke (1665) and Newton (1730). Continued and ever increasing interest, supported by the introduction of new investigation techniques, such as electron microscopy, has made it possible to discover countless examples of structural colour in nature, amongst both plants and animals. Feathers of many birds, for instance hummingbirds and peacocks, scales of fishes, setae of certain polychaete worms, retinal tissue of cats, and scales of butterflies are only a few examples of a phenomenon occurring across the animal kingdom, the existence of which during the last 515 million years is inextricably linked to the evolution of life (Parker 2000).

[†]Author for correspondence (luca.plattner@hitachigst.com).
Present address: Hitachi Global Storage Technologies, Inc., San Jose Research Center, 650 Harry Road, San Jose, CA 95120, USA.

The reader is referred to the excellent publications of Fox (1976), Land (1972) and Parker (2000) for reviews on this subject.

Amongst the many examples of structural colour found in nature, the beauty of the intense chromatic displays of butterflies has strongly captured the interest of researchers. The wings of butterflies are covered with elongated scales typically of the order of 100 μm in size, much in the fashion of a roof tiling. Typically, the top layer of a scale exhibits a regularly ridged structure, similar to a diffraction grating. An example of this structure is shown in figure 1. The lower parts of the scales usually contain pigments, either isolated in granules or dispersed throughout (Ghiradella 1984, 1985, 1991). The scales are made of dried cuticle, which is transparent and has an index of refraction of 1.56 at visible wavelengths (Land 1972; Vukusic 1999). The scales of butterflies exhibiting structural colour, often called *iridescent*, contain low amounts of pigments. The traditional classification of iridescent butterflies in two classes, with the recent addition of a third one (Vukusic *et al.* 2000), reflects the three fundamental architectures observed. In the first class, also called *Morpho* type, the ridges have the approximate shape of a pine tree in cross-section, their height is comparable to the distance between neighbouring ridges, i.e. the pitch

Received 21 April 2004
Accepted 7 July 2004
Published online 11 August 2004

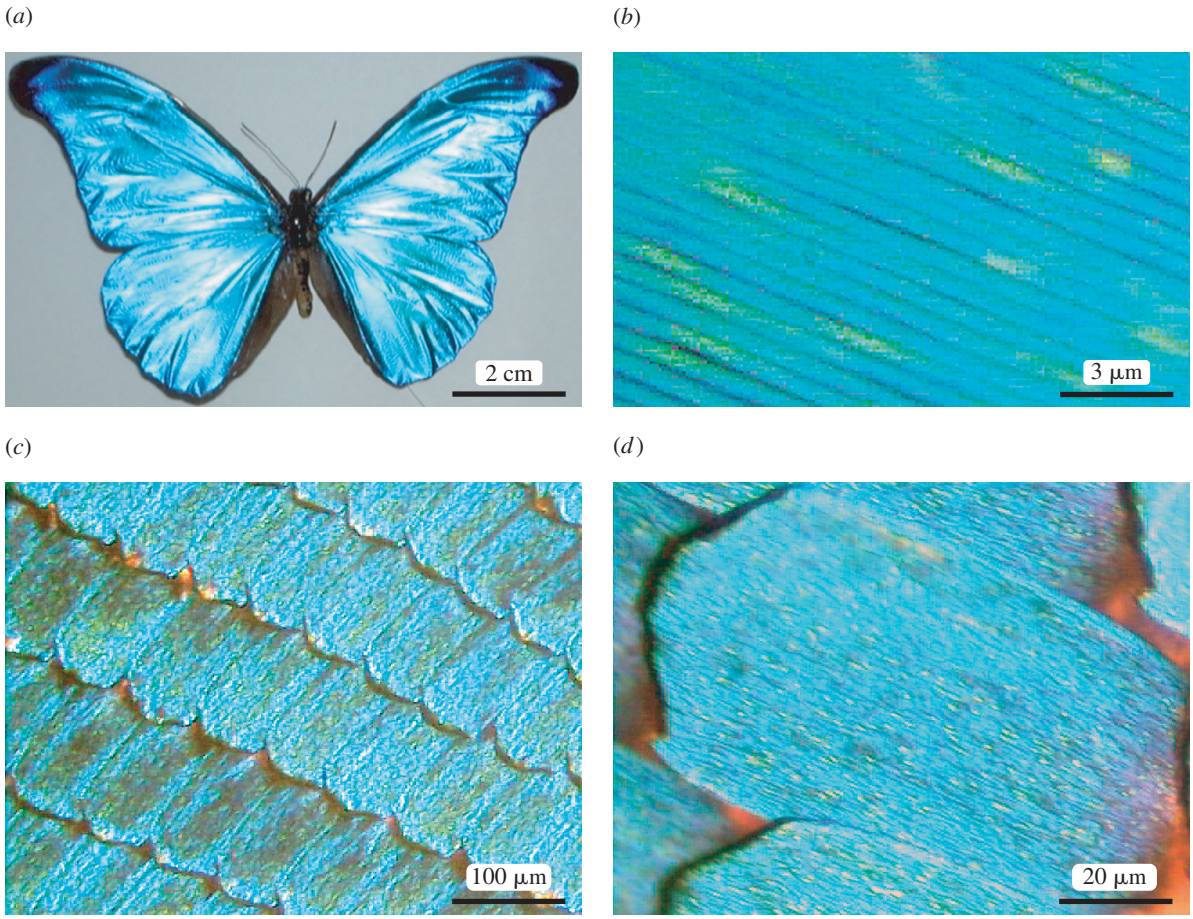

Figure 1. *M. rhetenor* (*a*) whole specimen, (*b*) detail of scale, (*c*) detail of wing and (*d*) scale.

of the grating, which is typically shorter than 1 µm, and much of the grating layer is filled with cuticle. The upper surface of the scales of butterflies belonging to the second class, also referred to as *Urania* type, is a multilayer, sometimes corrugated with a periodicity of several microns. The third class is characterized by an ordered, three-dimensional photonic crystal lattice of cuticle, which occurs within the scale. Figure 2 illustrates the cross-section of the surface microstructure found in a *Morpho*-type butterfly scale.

One species of tropical butterfly belonging to the first class, *Morpho rhetenor*, has attracted the interest of both zoologists and engineers in recent years, no doubt because of the striking brilliance of the blue colour shining from its wings. The intricate microstructure that covers the wings of this butterfly achieves, in the short wavelength regime of the visible spectrum, extremely high reflections of over 70% with a very large angular spread of the back-scattered light (Vukusic *et al.* 1999). While the mechanisms behind the phenomenology of *Urania*-type butterflies have been satisfactorily understood (Tada *et al.* 1999; Vukusic 2000), the models for *Morpho*-type butterflies have become increasingly more complex, passing from simple multilayers (Ghiradella *et al.* 1972) and multilevel gratings (Cowan 1990) through distributions of dielectric multilayers (Vukusic *et al.* 1999) to lamellar gratings (Gralak *et al.* 2001). Accordingly, the experimental investigation of their optical properties has become more complex and

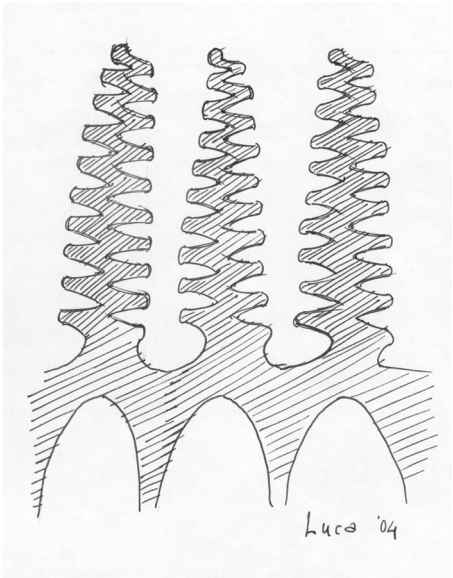

Figure 2. Cross-section of the upper surface in scales of *M. rhetenor*.

Vukusic *et al.* (1999) reported the most complete set of measurements yet of the optical properties of scales from a butterfly belonging to the first class, specifically *M. rhetenor*.

This paper reports a theoretical and experimental study of the microstructure found in the scales of *M. rhetenor*, which extends the knowledge gathered by previous scientists. A novel two-dimensional modelling tool that was developed for the theoretical analysis of periodic arrangements of dielectric found in the microstructure is presented in §2. An extensive characterization of the scattering of light by the scales of *M. rhetenor* for all visible wavelengths and polarizations and for various angles of incidence is reported in §3. A brief discussion of both theoretical and experimental results follows in §4.

The wings of *M. rhetenor* are tiled with a single layer of blue scales (cf. figure 1). These scales are typically $75 \times 200\,\mu m$ in size. On the upper surface they have a longitudinal ridging with an in-plane or horizontal periodicity of (675 ± 75) nm. The ridges have a pine-tree cross-sectional shape illustrated in figure 2, with approximately ten branches attached on both sides to a central stem, horizontal and regularly ordered, with a vertical thickness of about 90 nm. The thickness of the air interstices is also approximately 90 nm, which results in an average vertical periodicity of 180 nm. The cuticle fills *ca.* 30% of the volume occupied by the microstructure. The lamellae forming the branches of the tree structure are slanted along the direction of the ridges, with the angle of slant with respect to the plane of the wing at approximately 20°. The lower side of the scale is featureless and plain. Much of the mentioned geometrical data were obtained from electron microscopy studies published by Cowan (1990) and Vukusic *et al.* (1999).

2. THEORETICAL ANALYSIS

From optical and electron microscope analyses it appears that geometrical features such as the periodicity of the ridges, the thickness of the branches of the tree-shaped elements and their orientation are characterized by statistical distributions around average values with sizable variances. As in the example of quasicrystals (Zoorob *et al.* 2000) however, the occurrence of periodicity is central to the optical phenomenology of moderately disordered arrangements of dielectrics in their collective behaviour. The reported analysis abstracts from the study of such distributions and focuses on the effects of internal crystal structure and tapering of the tree-shaped elements. Models were drawn to approximate the irregular microstructure and they were designed to assess the role of two types of crystal lattice and of tapering in the generation of back-scattering. These models were two-dimensional, finite, periodic arrangements of rectangular slabs and are discussed in §2.2.

2.1. Methods

The finite-difference time-domain (FDTD) method of solving Maxwell's equations in two-dimensional, periodic and quasi-periodic arrangements of dielectrics with feature sizes comparable to the wavelength of the propagating radiation, e.g. mesoscopic structures and zero-order diffractive gratings, has emerged in recent years as a successful modelling tool. Scientists achieved accurate computation of several optical properties of these materials, from band structure (Chan *et al.* 1995) through Green's functions (Ward & Pendry 1998) to transmission coefficients (Zoorob *et al.* 2000).

The computational results presented here were obtained through propagation of a wavepacket impinging on dielectric models using the FDTD method, subsequent extraction of the scattered fields via a near-field to far-field transformation (NFFFT) in the time domain and final Fourier transformation to the frequency domain. The details of this method are discussed hereafter and the reader is referred to the books by Kunz & Luebbers (1993) and Taflove (1998) for introductions to these numerical techniques.

The FDTD computations were performed on an orthogonal and uniform grid. The nodes of the computation grid were 5 nm apart and time was stepped in intervals of 4×10^{-18} s, which yielded stable and accurate solutions in the visible spectrum. A fourth-order, staggered polynomial spatial difference scheme and a second-order time difference scheme were used. The algorithm incorporated smoothing of the interfaces between dielectrics and absorbing, perfectly matched layer (PML) boundary conditions, involving a split-field representation of the electromagnetic fields. The absorbing PML boundary consisted of 50 grid points surrounding the computation area. The initial condition was a pulse propagating along one of the grid axes with a Gaussian shape in the direction of propagation (Full Width at Half Maximum (FWHM) = 80 nm) and that of a supergaussian perpendicularly to it (FWHM = 2200 nm), which resulted in a wavepacket coherently propagating through the computation grid. The use of absorbing boundary conditions with a finite initial pulse, as opposed to periodic boundary conditions and an infinitely wide incident field, allows one to model the finiteness of the volume in which the interaction between light and the diffractive structures takes place. A schematic of the components of a typical computation is given in figure 3*a*. The computations for transverse electric (TE) polarized fields, i.e. having the electric field oriented perpendicularly to the incidence and computation plane, and transverse magnetic (TM) polarized ones, i.e. having the magnetic field oriented perpendicularly to the incidence and computation plane, were performed separately. Different angles of incidence were implemented by changing the orientation of the dielectric with respect to the direction of propagation of the initial wavepacket, which was kept constant. Figure 3*b* shows an intensity plot of a computation field after 250 time steps from its beginning; the propagating wavepacket and the scattered fields are clearly visible.

The scattered fields were sampled at points of the grid 500 nm (100 grid points) away from the edges of the computed zone along four straight windows resulting in a closed rectangle. Solution of the Fresnel–Kirchhoff integral in its full vectorial form permits extraction of the far-field representation of the scattered fields. This was achieved numerically through NFFFT performed in the time domain on the sampled data from each window for directions of propagation at intervals of 1° over the whole scattering hemicycle of a window.

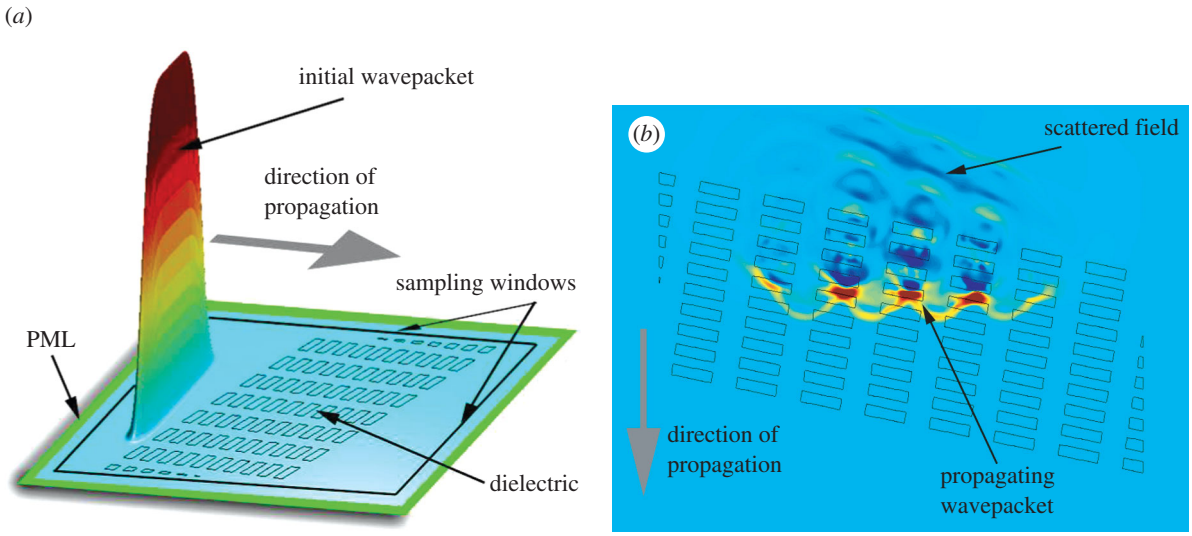

Figure 3. (*a*) Schematic of a typical computation including the computed area, dielectric, initial wavepacket, sampling windows and perfectly matched layer boundary. (*b*) Intensity plot of a computation field after 250 time steps from its beginning.

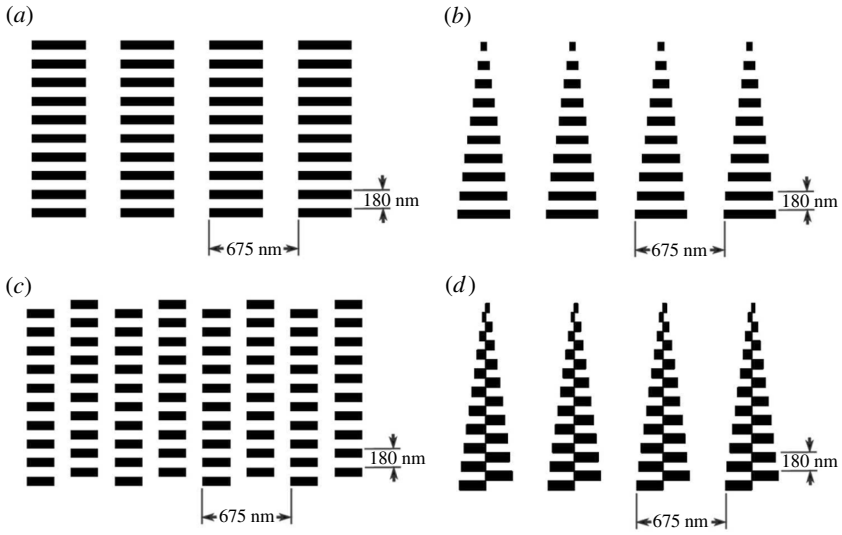

Figure 4. Schematics of the dielectric models studied numerically: (*a*) model (i) a rectangular lattice of rectangular dielectric elements; (*b*) model (ii) a tapered version of (i), resulting in a pine-tree structure with its tips towards the incident front; (*c*) model (iii) a centred rectangular lattice of rectangular dielectric elements; (*d*) model (iv) a tapered version of (iii), resulting in an asymmetric pine-tree structure.

Then, dividing the reciprocal space into four quadrants with respect to the orthogonal directions of the grid, the contributions to the field flux in each direction of propagation from neighbouring sampling windows were added for each quadrant. Successively, the fields were Fourier transformed which yielded data exhibiting a spectral resolution smaller than 3 nm in the visible range of wavelengths. Finally, absolute values for the field intensities were obtained by normalization of the power densities by the sum of all the power scattered in the completely computed cycle of directions.

All computations were performed on 32bit personal computers having 256 MB of RAM. The computational tool was compared with results published by Sakoda (1995) on materials comparable to the *Morpho* microstructure (triangular lattices of air cylinders in a low-index dielectric slab) and obtained using expansion methods, which proved to describe accurately the properties of fabricated optical nanostructures in the frequency range of interest (Labilloy *et al.* 1997). The two methods agree within 1.3% with respect to the central frequency of a band of strongly backscattered light, called a *bandgap*, and within 12.9% with respect to its FWHM.

2.2. Results

Using the computational tool presented in §2.1, four different models incorporating patterns occurring in the *Morpho* microstructure and shown in figure 4, were

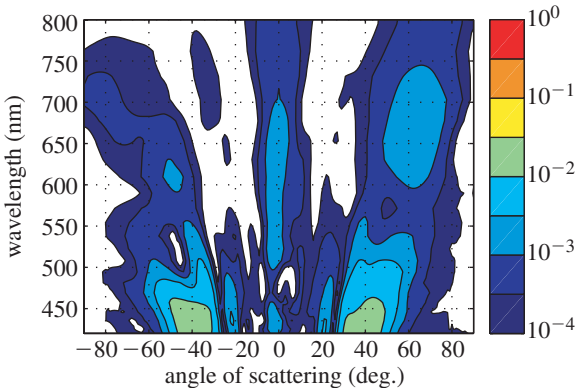

Figure 5. Filled contour plot of the computed back-scattering of the tapered centred rectangular model (iv) for TM polarized light impinging normally. Colour coded intensities are represented in a logarithmic scale.

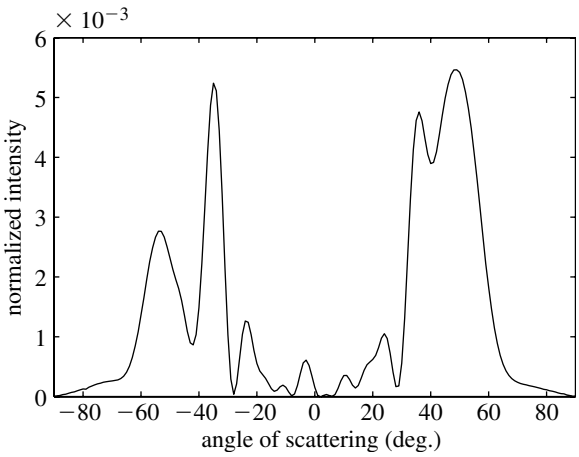

Figure 6. Computed angular distribution of the back-scattering at 488 nm for TM polarized light when impinging normally on model (iv). This is a cross-section of the plot shown in figure 5.

studied numerically. All models were composed of one dielectric having an index of refraction of 1.56 embedded in vacuum (or air). In this way, absorption was neglected, which, however, only affects the magnitude of waves and not their optical pathlengths, and therefore does not influence the interference mechanisms. The structures were: model (i) a rectangular lattice of rectangular dielectric elements; model (ii) a tapered version of (i), resulting in a pine-tree shaped structure with its tips towards the incident front; model (iii) a centred rectangular lattice of rectangular dielectric elements; model (iv) a tapered version of model (iii), resulting in an asymmetric pine-tree shaped structure. While models (i) and (ii) share the same lattice and so do (iii) and (iv), models (i) and (iii) share the same area filling fraction (30%) and so do (ii) and (iv), namely 16.75%. The models are shown in figure 4. Periods and dimensions of these models were chosen both from optical microscopy and published electron microscopy data (Cowan 1990 and Vukusic *et al.* 1999).

The intensity of the light back-scattered from model (iv) when the wavepacket impinges normally and for the TM polarization is shown in the spectrogram of figure 5, which consists of a colour coded, filled contour plot on a logarithmic scale. On the axes are the direction of propagation with respect to the normal to the structure surface, and the wavelength of the scattered field. We observe strong extinction of the specular reflection (0°) and, for short wavelengths in the visible spectrum, a distribution of the back-scattered light in two lobes around the ±40° directions (green patches). A cross-section along the 488 nm wavelength is shown in figure 6. A similar distribution has previously been measured at this wavelength on scales of *M. rhetenor* and was reported by Vukusic *et al.* (1999). It is necessary to clarify that while the lobes in the computed spectra are generated by the angular spread of the diffracted orders due to the finite number of diffraction elements involved in the process, in measurements on the scales the presence of a range of periods and of Rayleigh scattering at individual features in the ridged arrangement are expected to be mainly responsible for the formation of the lobes.

Such computations were performed on all the models mentioned above for both polarizations and for angles of incidence of 10°, 30° and 60°, which were chosen as representative directions of the whole hemicycle of incidence in both the theoretical and the experimental analysis. The results were analysed by extracting the spectra of the total reflection via summation of all back-scattered power at each wavelength in the spectrum. These spectra are shown in figure 7 for all models and angles of incidence, and for the TE polarization.

For the structures on a rectangular lattice (models (i) and (ii)), most of the back-scattered power is found at wavelengths shorter than 530 nm and 510 nm at both angles of incidence of 10° and 30° and for the TE and TM polarization, respectively. For the structures on a centred rectangular lattice (models (iii) and (iv)) on the other hand, most of the back-scattered power is found at wavelengths shorter than 490 nm and 460 nm at both angles of incidence of 10° and 30° and for the TE and TM polarization, respectively. In all cases total reflections larger than 58% are achieved for 10°, with maximum values of up to 96%. For both lattices, a tapering of the diffraction elements (models (ii) and (iv)) causes lower reflection at long wavelengths in the visible spectrum and a suppression of local modulation, which results in smoother and wider peaks.

These results compare favourably with band calculations performed using expansion methods. For the benefit of the reader familiar with these methods, but without wanting to go into too much detail, a brief description follows. We computed the upper edge of the band in the first Brillouin zone for both a rectangular and centred rectangular lattice as used in the FDTD calculations (models (i) and (iii)), but infinitely extended. To achieve this we used a two-dimensional plane-wave expansion method with 81 terms in both the field and dielectric function expansions. This edge was found to be very flat in both cases (i.e. constant for a variety of angles of propagation) and for the rectangular lattice it is at wavelengths of 500 nm and 482 nm, for TE and TM polarizations respectively, while

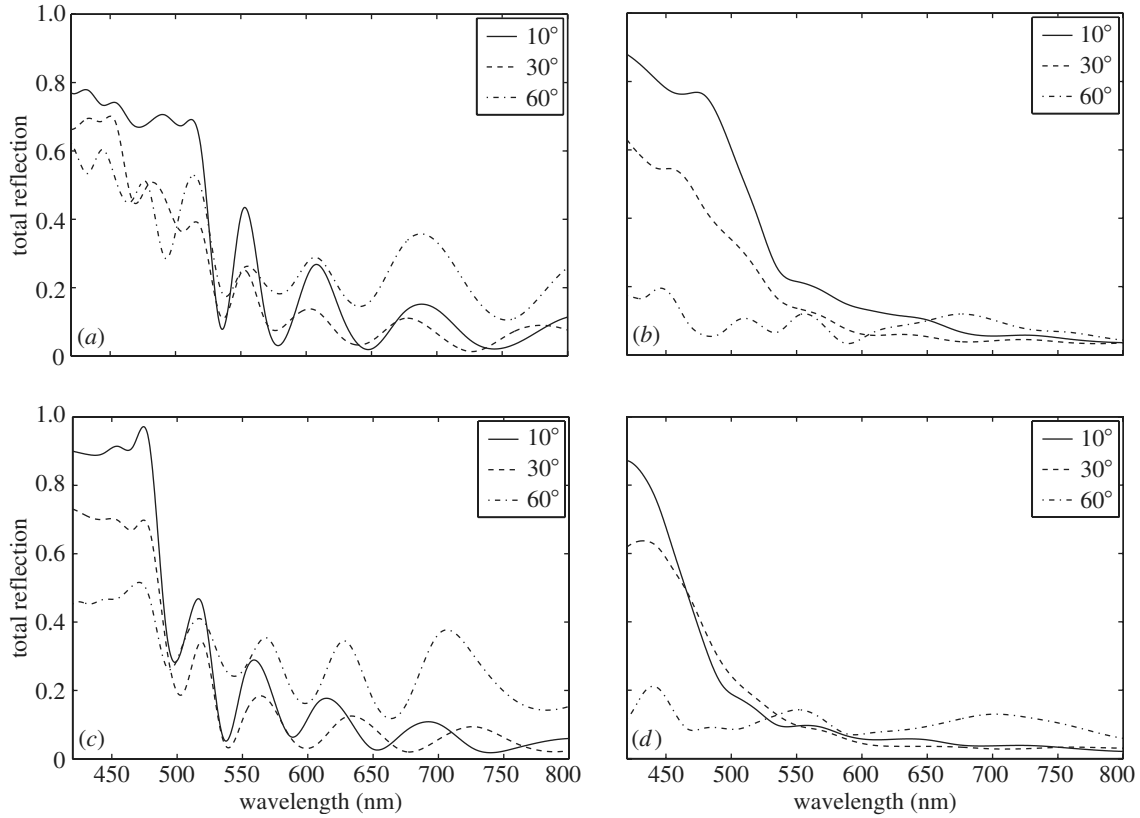

Figure 7. Computed spectra of the total reflection for TE polarization and angles of incidence in models (i)–(iv). The lettering corresponds to that of figure 4.

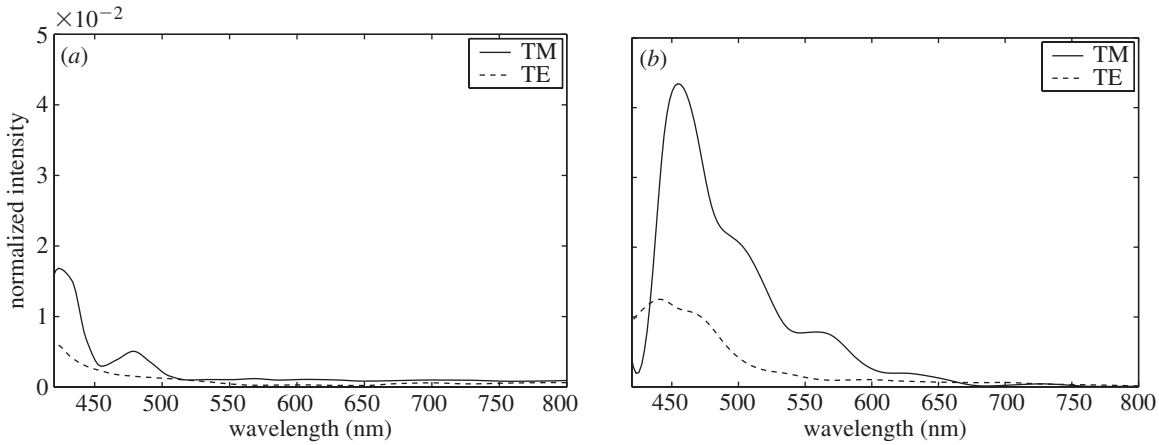

Figure 8. Computed diffraction efficiencies of model (ii) for a 30° angle of incidence and both polarizations. Graph of the (*a*) zeroth order of diffraction (specular reflection) and of (*b*) the first order of diffraction.

for the centred rectangular lattice it is at 466 nm and 432 nm, for TE and TM polarizations respectively. The values for infinitely extended models are systematically smaller than the ones from the finite FDTD modelling, an expected effect related to the sharper peaks caused by the interference of a larger number of waves.

Additionally, the diffraction of light by the models in the back-scattering domain was analysed. The organization of the back-scattered power in orders of diffraction, apparent from all spectrograms, as in the one of figure 5 and responsible for the occurrence of the mentioned lobes, was quantified by extracting the scattered intensity along the theoretical diffraction curves using polynomial interpolation. An example of diffraction efficiencies is given in figure 8, where, for computations performed on model (ii) with a wavepacket impinging at 30°, the field intensities have been extracted for the zeroth order of diffraction (specular reflection, 30°) and for the first (−10° at 455 nm), shown in graphs (a) and (b), respectively.

From such analysis, we conclude the following.

- Model (iii) shows a strong extinction of the specular reflection with respect to the first order of diffraction for the smaller angles of incidence and both polarizations (with extinction ratios larger

than −18 dB for an angle of incidence of 30° at 420–450 nm), which does not occur in model (i).
- Tapering in models (ii) and (iv) enhances the distribution of the back-scattered power to the first order of diffraction when spectra are compared to models (i) and (iii), respectively. This causes model (iv) to show the highest extinction of specular reflection, with extinction ratios larger than −19 dB.
- Tapering also causes the elimination of all minor modulation of the spectra observed in non-tapered models, thus leaving only one or two large peaks in the whole visible spectrum.

Finally, the effect of varying the lateral and vertical periods of the models was also studied. A change in lateral period (with variations between 525 and 825 nm) causes the expected shift of the lobes according to the changed diffraction condition. In the total reflection spectra however, although a variation of the maxima of the main peak is observed consistently with the varying filling fraction, no substantial change is found in the position of the long-wavelength edge of this peak, which shifted within 5 nm. For the variations of vertical period the long-wavelength edge of the total reflection peaks is equally unchanged when the wavelength is normalized to the period. All our calculations are in fact scalable and both variations are effectively equivalent.

3. EXPERIMENTAL ANALYSIS

Surface coupling techniques have recently emerged as important tools for the experimental investigation of mesoscopic periodic materials (Astratov *et al.* 2000; Netti *et al.* 2001). The coupling of impinging light to their photonic bands shows up in reflectivity spectra, which allows for the extrapolation of optical properties related to the band structure and periodicity of the devices, such as their dispersion.

Using our generic knowledge of the microstructures found on the wings of *M. rhetenor*, an experimental setup was built to characterize their back-scattering of visible light by spectroscopy, with the aim to confirm and quantify the diffractive behaviour expected from the theoretical analysis.

A photonic crystal fibre (PCF) was employed to provide a mobile source of coherent white light, which permitted us to focus a high intensity beam containing all the wavelengths of the visible spectrum on a single scale. Thus, effects deriving from the coincident illumination of several scales, such as microstructure misalignments and diffraction at the edges of a scale, could be eliminated and also the availability of an intense source permitted the use of a fast and inexpensive spectrometer. The properties and use of the PCF will be discussed below.

First, by illuminating the scales with the white light and projecting their back-scattered light on a screen the two-dimensionality of the microstructure was confirmed. In fact, a grating-like scattering pattern consisting of a single straight line, typical of a two-dimensional structure, was verified in all the members of a large sample of investigated scales and in a variety of conditions of incidence. This acknowledgement was the basis for the design of the experimental setup described hereafter.

3.1. Methods

A 2 m-long piece of silica PCF with a nominal core diameter of 2 µm and a total diameter without cladding of 125 µm was pumped with a high-power, ultrashort infrared (IR) pulsed signal obtained by a regenerative titanium sapphire (Ti:Sa) amplified laser source. This produced an 800 nm wavelength seed for the supercontinuum (SC) generation in the PCF, having a pulse width of 150 fs (FWHM), a repetition frequency of 250 kHz and a time-averaged power of 10 mW, which corresponds to a peak power of 26.7 kW and an energy per pulse of 4 nJ. The IR beam was coupled into the PCF using a 60× microscope objective and a high-accuracy *xyz* positioning stage. Figure 9*a* shows a SEM cross-sectional view of the PCF.

This source provided an excellent white light SC, comparable in quality to results from published work (Ranka *et al.* 2000; Genty *et al.* 2002; Price *et al.* 2002), supplying a reliable and flexible mobile source for experiments which require a prolonged operation. The spectrum of the SC optimized for visible applications and stretching from 400 to 900 nm is shown in figure 9*b*.

The output end of the PCF was mounted on the incidence arm of a specially designed goniometer, which through a conical ring and shaft design, the use of high-quality materials and precision machining allowed us to position the incidence beam on the samples with an accuracy of a few microns while varying the angle of incidence over the whole hemicycle.

For the following description of the experimental setup the reader is invited to refer to the schematic of figure 10. The white SC escaping the PCF's output was collimated using a 40× objective and the moderate polarization of the beam was made complete with a Glan–Taylor polarizer (GT). The orientation of the linear polarization of the beam was then controlled via a $\lambda/2$ plate and the IR spectral content reduced with a high-pass filter (KG1). About 10% of its power was then removed for referencing purposes with an achromatic filter (inconel-NiCrFe ND 0.1) and once focussed, it was collected by one branch of a bifurcated optical fibre attached to the incidence arm and feeding into the spectrometer. The low-aperture (6×10^{-4} srad) incident beam was focussed to a beam-waist of (30 ± 5) µm (FWHM) projected onto the sample by a 0.5 in achromatic lens with a focal length of 75 mm. In this way we could ensure that the incident beam was contained well within the investigated scales. Once a condition of incidence was selected, the sample was kept fixed with the incidence arm of the goniometer.

The light scattered by the sample in the plane of incidence was collected over a solid angle determined by an iris mounted on the optical table and the direction of collection was varied by changing the direction of the incidence arm of the goniometer. The aperture of the collected beam was 0.64 srad. The beam was collimated, its polarization controlled with a further polarizer and a $\lambda/2$ plate, attenuated to a suitable intensity, and finally

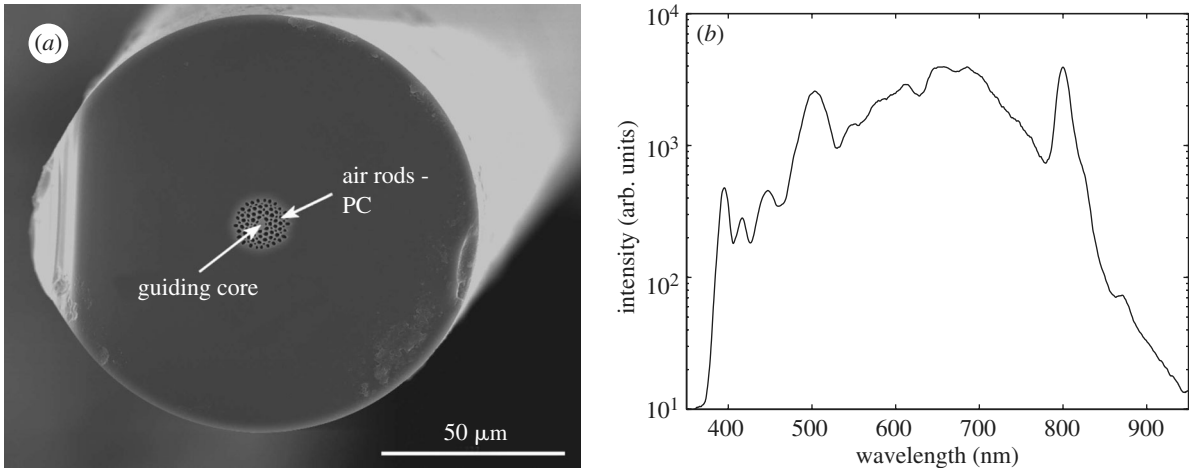

Figure 9. (*a*) SEM cross-sectional view of silica photonic crystal fibre without external cladding (reproduced courtesy of W. Belardi, ORC, University of Southampton). (*b*) Spectrum of supercontinuum obtained from PCF.

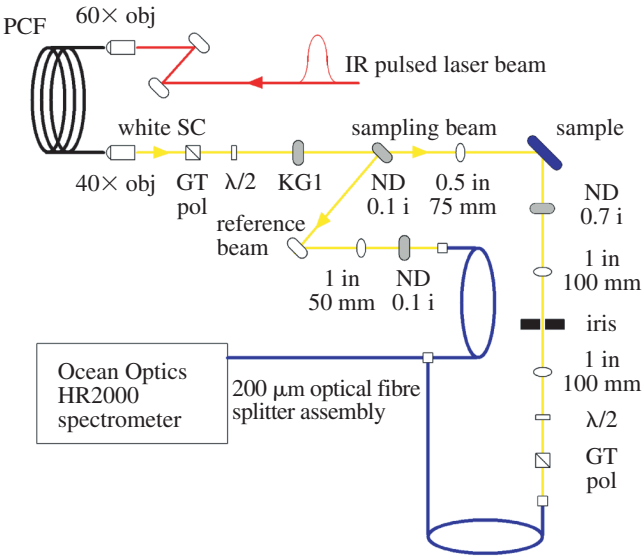

Figure 10. Schematic of the experimental setup.

focussed onto the second branch of the optical fibre feeding into the spectrometer. All the optics involved were achromatic to exploit optimally the white light source and minimize aberration. The high-resolution spectrometer was an Ocean Optics HR2000, with a 10 µm slit, a 300 l mm^{-1} grating and a resolution of 1 nm, and was connected to via a splitter assembly of 200 µm core, single strand optical fibres. The light scattered from the surface of a sample could be measured over nearly 180°, with the exception of a blind spot, an arc extending ±10° from the direction of the incident beam which was due to a limitation in movement of the incidence arm caused by the collection optics.

A small portion of a wing was attached to a flat surface and fixed in the sample holder. The ridges of the microstructure were oriented parallel to the axis of rotation of the goniometer, such as to be normally oriented with respect to the plane of incidence. This was achieved by projecting the scattered field onto a cylindrical screen, which resulted in a horizontal line, when the wing was inclined at an approximate angle of 20° due to the slanting of the layering and the tilt of the wing substrate.

A measurement of the reference beam was performed immediately before and after each acquisition of scattering data in order to minimize the effects of fluctuations in the spectral content of the incident beam and obtain accurate relative measurements. Each acquired spectrum was also corrected for intrinsic achromaticity of the setup, gauged through reflection measurements of a high-quality mirror.

By performing the measurements at angles of scattering between the grazing angle on one side of the wing normal to the grazing angle on the other side we ensured that the surface of the microstructure was oriented within an accuracy of ±5° from the expected direction.

3.2. Results

Measurements were performed for angles of incidence of 10°, 30° and 60°. The polarization of the incident and scattered beams was either parallel (TM) or perpendicular (TE) to the plane of incidence. No noticeable effects of cross-polarization of the scattered field were detected at any of the investigated angles of incidence.

The back-scattered light intensity was measured at directions 5° apart and covering all the directions in the plane of incidence between −85° and 85° with the exception of the blind spot of the measurement setup. For each angle of incidence and polarization, a total of thirty spectra were collected and the closest measurements to the path of incidence were 15° away from it in the plane of incidence. Since the solid angle of collection corresponded to a cone with a slope of about 2.5°, the scattered light was sampled with a high angular resolution without any gaps left other than the blind spot. Figure 11 shows filled contour plots of all the measurements with the angle of scattering and the light wavelength as coordinates, where the colour-coded intensity of the two-dimensional scattering spectrogram is scaled to the reflection of a high-quality achromatic mirror representing the value 1 and the

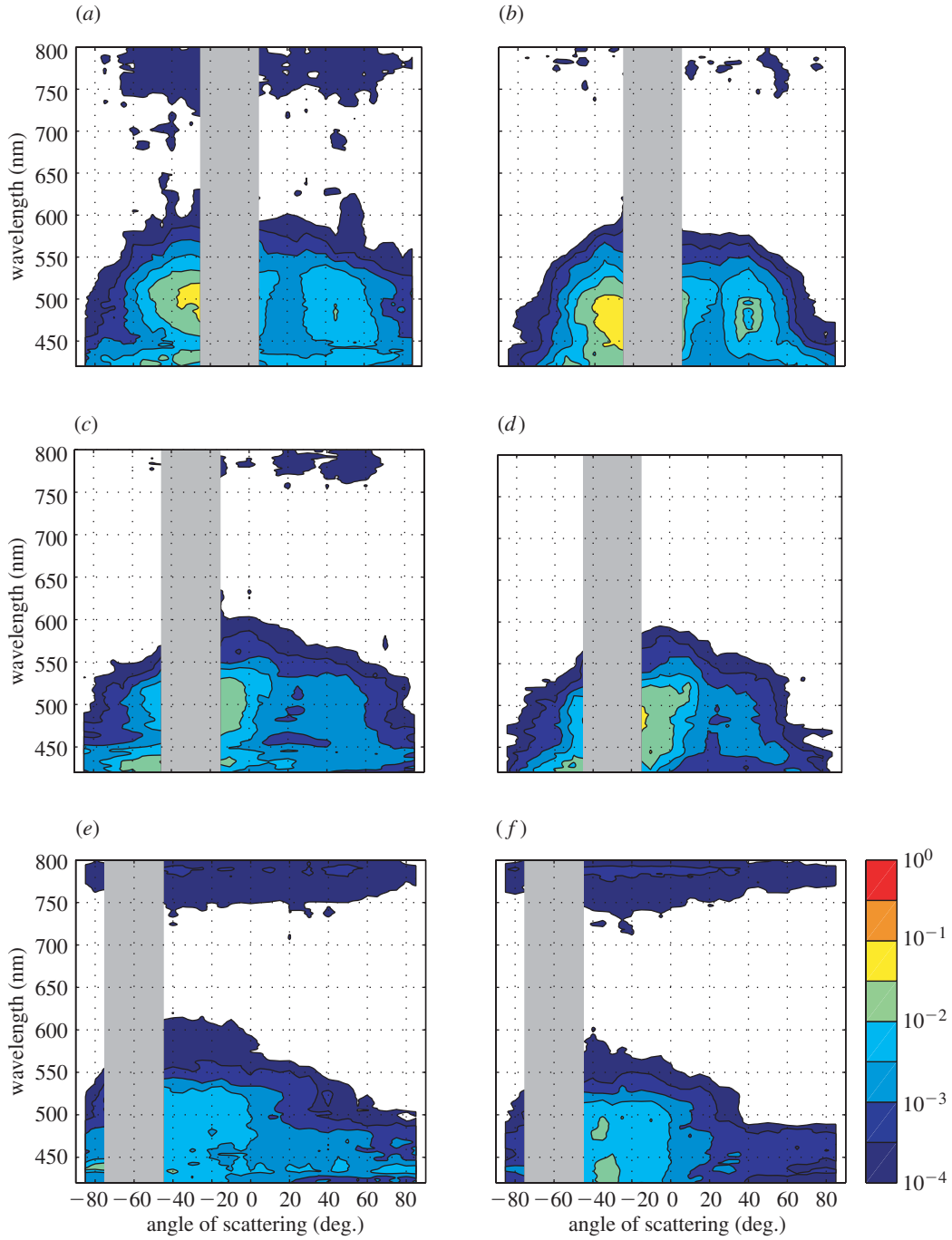

Figure 11. Filled contour plots of the scattering off the surface of the wings of *M. rhetenor* at different angles of incidence and polarization: (*a*) and (*b*) 10° incidence, (*c*) and (*d*) 30° incidence, (*e*) and (*f*) 60° incidence; (*a*), (*c*) and (*e*) TE polarization, (*b*), (*d*) and (*f*) TM polarization. The grey areas correspond to the blind spot of the measurement setup.

intensity is plotted on a logarithmic scale. The grey areas correspond to the blind spot of the setup.

By summing the spectra for all the angles of scattering one obtains the total reflections of the microstructure, which are shown in figure 12. The majority of the scattered power is found at wavelengths shorter than 550 nm, with the longer wavelengths being highly transmitted by the microstructure. For different polarizations similar distributions of power are found in the spectrograms with different patterns locally. In general, the wing microstructure acts as a retro-reflector irrespective of the orientation of its surface, with most of the scattered power found at angles close to the incident one. At an incident angle of 10°, two lobes are found in the angular distribution of the scattered power, one located around 40° and one approximately around −20°, the second more intense than the first. At the higher angles of incidence, the lobe in the positive range of angles disappeared, the overall intensity of the stronger features decreased with increasing angle of incidence and the lobe in the negative range of angles is split in two. Also, at all angles of incidence the angular spreading of the lobes is increased with decreasing wavelengths and, for the TE polarization,

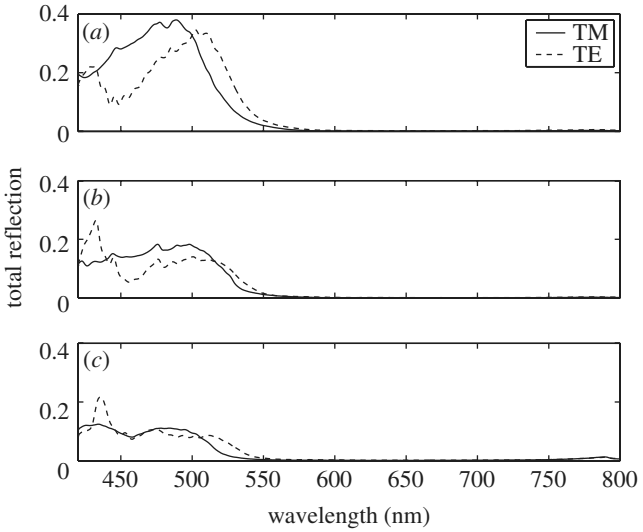

Figure 12. Total reflection of *M. rhetenor* microstructure for angles of incidence of (*a*) 10°, (*b*) 30° and (*c*) 60°, and both polarizations.

a background band of constant intensity extends over most of the measured range of angles for wavelengths around 430 nm, where part of the split lobe is centred. For an angle of incidence of 60°, more light is back-scattered at longer wavelengths, again forming a band extending over a wide angular range.

It is apparent from the spectrograms that interesting information has been lost to the blind spot due to the general behaviour of the microstructure as a retro-reflector. Although modifications to the experimental setup to reduce the extent of the blind spot are conceivable, they required a major redesign which was not implemented at this stage. Elimination of the blind spot can ultimately only be achieved through coinciding incidence and collection paths. Nevertheless, the observed properties shed new light on the mechanisms of colour production in the microstructure and support the findings of the theoretical analysis.

4. DISCUSSION

It has been demonstrated experimentally that the scales of *M. rhetenor* act as low-pass filters of visible light for angles of incidence throughout most of the incidence hemicycle. The spectral content of the back-scattering of white light for all investigated angles of incidence is exclusively at wavelengths shorter than 550 nm, which quantitatively confirms the observed blue colouration of the butterfly wings in accordance with the CIE standard observer colour matching functions (Stiles & Burch 1959). The back-scattered light in its angular representations (cf. spectrograms) is organized in lobes, the position of which depends on the angle of incidence. Also, a strong extinction of the specular reflection was observed, with a marked retro-reflector behaviour for angles of incidence of 30° and above.

These experimental findings are consistent with the two-dimensional theoretical analysis, in which four geometrical periodic arrangements designed after the microstructure were modelled numerically. All these idealized models exhibit a strong spectral filtering similar to that measured experimentally and would appear blue at all investigated angles of incidence. The relative positions of the omnidirectional thresholds for the two polarizations are equally consistent, while their absolute values can be made to match the experimental ones through scaling of the models by only a few percent.

The diffraction of the grating-like periodic models also correctly predicts, within the limitations of their idealization, the organization of the back-scattering in lobes, suggesting that the diffraction of reflected light is an important mechanism behind the phenomenology of the microstructure. The occurrence within the microstructure of a centred rectangular lattice was shown to potentially explain the extinction of the specular reflection. The tapering of the elements further enhances the retro-reflector phenomenology for both types of lattice, the rectangular and the centred rectangular one, due to the extinction of diffraction observed in the positive regimes of scattering angles.

However, the author would like to point out here that it is not possible to establish a conclusive causal link between the modelling and observations. The overall response of the butterfly microstructure to illumination is the result of a variety of factors, such as the mentioned distribution of periodical features and the irregular shape of each individual feature, both difficult to quantify.

This work has been supported by and carried out at the University of Southampton. The invaluable contribution of Dr M. E. Zoorob for the reported computational study is acknowledged, as well as the germinal input of Professor G. J. Parker and constructive discussions with Dr M. C. Netti, Professor J. J. Baumberg and Dr A. R. Parker. All of the above are with the University of Southampton, with the exception of Dr Parker, who is with Oxford University. Thanks to Dr W. Belardi of the Optoelectronics Research Centre, University of Southampton for providing an excellent sample of photonic crystal fibre.

REFERENCES

Astratov, V. N., Stevenson, R. M., Culshaw, I. S., Whittaker, D. M., Skolnick, M. S., Krauss, T. F. & De La Rue, R. M. 2000 Heavy photon dispersions in photonic crystal waveguides. *Appl. Phys. Lett.* **77**, 178–180.

Chan, C. T., Yu, Q. L. & Ho, K. M. 1995 Order-N spectral method for electromagnetic waves. *Phys. Rev.* B **51**, 16635–16642.

Cowan, J. J. 1990 Aztec surface-relief volume diffractive structure. *J. Opt. Soc. Am.* A **7**, 1529–1544.

Fox, D. L. 1976 *Animal biochromes and structural colours.* Cambridge University Press. (Reprinted by Berkeley University Press, 1976.)

Genty, G., Lehtonen, M., Ludvigsen, H., Broeng, J. & Kaivola, M. 2002 Spectral broadening of femtosecond pulses into continuum radiation in microstructured fibers. *Opt. Expr.* **10**, 1083–1098.

Ghiradella, H. 1984 Structure of iridescent lepidopteran scales: variation on several themes. *Ann. Entomol. Soc. Am.* **77**, 637–645.

Ghiradella, H. 1985 Structure and development of iridescent lepidopteran scales: the papilionidae as a showcase family. *Ann. Entomol. Soc. Am.* **78**, 252–264.

Ghiradella, H. 1991 Light and color on the wing: structural colors in butterflies and moths. *Appl. Opt.* **30**, 3492–3500.

Ghiradella, H., Aneshansley, D., Eisner, T., Silberglied, R. E. & Hinton, H. E. 1972 Ultraviolet reflection of a male butterly: interference color caused by thin-layer elaboration of wing scales. *Science* **178**, 1214–1216.

Gralak, B., Tayeb, G. & Enoch, S. 2001 Morpho butterflies wings color modeled with lamellar grating theory. *Opt. Expr.* **9**, 567–578.

Hooke, R. 1665 *Micrographia*. London: The Royal Society. (Reprinted by Palo Alto: Octavo, 1998.)

Kunz, K. S. & Luebbers, R. J. 1993 *Finite difference time domain method for electromagnetics*. Boca Raton, FL: CRC Press.

Labilloy, D., Benisty, H., Weisbuch, C., Krauss, T. F., De La Rue, R. M., Bardinal, V., Houdré, R., Oesterle, U., Cassagne, D. & Jouanin, C. 1997 Quantitative measurement of transmission, reflection, and diffraction of two-dimensional photonic band gap structures at near-infrared wavelengths. *Phys. Rev. Lett.* **79**, 4147–4150.

Land, M. F. 1972 The physics and biology of animal reflectors. *Prog. Biophys. Mol. Biol.* **24**, 75–106.

Netti, M. C., Harris, A., Baumberg, J. J., Whittaker, D. M., Charlton, M. D. B., Zoorob, M. E. & Parker, G. J. 2001 Optical trirefringence in photonic crystal waveguides. *Phys. Rev. Lett.* **86**, 1526–1529.

Newton, I. 1730 *Opticks*, 4th edn. London: William Innys. (Reprinted by New York: Dover, 1952.)

Parker, A. R. 2000 515 million years of structural colour. *J. Opt. A: Pure Appl. Opt.* **2**, R15–R28.

Price, J. H. V., Belardi, W., Monro, T. M., Malinovski, A., Piper, A. & Richardson, D. J. 2002 Soliton transmission and supercontinuum generation in holey fiber, using a diode pumped Ytterbium fiber source. *Opt. Expr.* **10**, 382–387.

Ranka, J. K., Windeler, R. S. & Stentz, A. J. 2000 Visible continuum generation in air-silica microstructure optical fibers with anomaluos dispersion at 800 nm. *Opt. Lett.* **25**, 25–27.

Sakoda, K. 1995 Transmittance and Bragg reflectivity of two-dimensional photonic lattices. *Phys. Rev.* B **52**, 8992–9002.

Stiles, W. S. & Burch, J. M. 1959 NPL colour-matching investigation: final report. *Optica Acta* **6**, 1–26.

Tada, H., Mann, S. E., Miaoulis, I. N. & Wong, P. Y. 1999 Effects of a butterfly scale microstructure on the iridescent color observed at different angles. *Opt. Expr.* **5**, 87–92.

Taflove, A. 1998 *Advances in computational electrodynamics: the finite-difference time-domain method*. Norwood, MA: Artech House.

Vukusic, P. 2000 Colour mixing in wing scales of a butterfly. *Nature* **404**, 457.

Vukusic, P., Sambles, J. R., Lawrence, C. R. & Wootton, R. J. 1999 Quantified interference and diffraction in single *Morpho* butterfly scales. *Proc. R. Soc. Lond.* B **266**, 1403–1411.

Vukusic, P., Sambles J. R. & Ghiradella. H. 2000 Optical classification of microstructure in butterfly wing-scales. *Photonics Science News* **6**, 61–68.

Ward, A. J. & Pendry, J. B. 1998 Calculating photonic Green's functions using a nonorthogonal finite-difference time-domain method. *Phys. Rev.* B **58**, 7252–7259.

Zoorob, M. E., Charlton, M. D. B., Parker, G. J., Baumberg, J. J. & Netti, M. C. 2000 Complete photonic bandgaps in 12-fold symmetric quasicrystals. *Nature* **404**, 740–743.